Biodegradable Composites Based on Well-characterized Cellulose and Poly (Butyleneadipate-Co-Terephthalate)

Peipei Li,[a] Yiqing Qin,[a] Qi Xu,[a] and Guichang Jiang [a,b,*]

As a biodegradable and flexible copolymer, poly(butyleneadipate-co-terephthalate) (PBAT) is used for packaging. However, high cost and limited properties restrict its applications. Because of the hydrophobic nature of PBAT, low mechanical properties are observed when PBAT and cellulosic fibers, which are hydrophilic, are used in blends. To increase the interfacial adhesion between cellulose and PBAT, γ-(2,3-epoxypropoxy) propytrimethoxysilane (KH560) was used as a reactive compatibilizer to modify cellulose. A one-step method was demonstrated for compounding and subsequent extrusion blowing, which is a simple and environmentally friendly approach to fabricate a series of K-Cellulose/PBAT (KH560-Cellulose/PBAT) composites. The morphology and structure of the cellulose were characterized by scanning electron microscopy, X-ray diffraction, and Fourier transform infrared spectrophotometry. Meanwhile, thermal analysis of the hybrids showed an improvement of the thermal stability of the composites with increased silanized cellulose content. In addition, the barrier properties of films are measured by water vapor permeability (WVP) and oxygen permeability (OP). Finally, after addition of reactive compatibilizer KH560, there was considerable improvement with increased the cellulose content, as shown through mechanical properties testing. Therefore, the composites prepared with these enhanced properties have great potential as substitutes for traditional commodity polymers.

DOI: 10.15376/biores.18.1.1916-1932

Keywords: Cellulose; Poly butylene terephthalate; Biodegradable film; Extrusion blowing

Contact information: a: Tianjin University of Science & Technology, Tianjin, 300222, People's Republic of China; b: Dept. of Chemistry, Tsinghua University, Beijing 100084, People's Republic of China;
** Corresponding author: gcj@tust.edu.cn*

INTRODUCTION

Changes in consumption habits over the past 50 years have increased the quantity of disposable or short-lived items, such as packaged commodity polymers (Adam *et al*. 2013). For example, the plastic film market is dominated by these polymers with multiple properties that cannot be biodegradable and take hundreds of years to decompose in nature after treatment (Bodros *et al*. 2007; Cao *et al*. 2020). Thus, to reduce environmental pollution from traditional plastics, many great efforts have been made to develop environment-friendly biodegradable materials (Cao *et al*. 2020). It is inevitable to think about the substitution of such polymers by biodegradable ones in many applications.

Polybutylene adipate-co-terephthalate (PBAT) is a flexible and biodegradable polymer. It has received the biodegradable and compostable material certification seal, given by European Bioplastics (EN 13432 (2020) standard criteria) and by the Biodegradable Polymers Institute (ASTM D6400 (2020) standard specification) (Cao *et al*.

2020). Nonetheless, to increase its range of use, it is important to improve some of its properties, including mechanical strength and barrier properties. For instance, this improvement can be achieved through cellulose reinforcement fillers (Da Costa *et al.* 2019). Enhanced PBAT composites using biological nanoparticles is an effective method (Darshan *et al*. 2019). Recent studies have reported that cellulose nanowhiskers (CNW) have excellent thermal and mechanical properties with a large length-to-width ratio (Edlund *et al*. 2019), high strength, and suitability for forming elastic modulus-enhanced PBAT composites (Fukushima *et al*. 2012).

Bamboo grows in many tropical areas of the world, especially in Zhejiang Province, China (Higbee-Dempsey *et al*. 2020). Because of the preponderance of fast growth rate, high strength, high surface hardness, and easy processing, it is widely used in furniture manufacturing, building materials, and for the production of household goods (Jin *et al*. 2019). However, a large amount of bamboo processing residues are underutilized. Bamboo has an equivalent cellulose content to that of wood, ranging from 40% to 65% (Li *et al*. 2015; Kim and Cho 2020). Therefore, bamboo residues can serve as a good resource for renewable nanobio-based fillers (Lin *et al*. 2018). Some researchers (Mhd Ramle *et al*. 2020) hydrolyzed bamboo fibers, such as to form cellulose nanocrystals (CNCs) in the presence of sulfate and phosphate. These CNCs had lengths of approximately 100 nm. Bamboo cellulose has been used as an enhancer in rubber composites. Oliveira *et al.* (2017) found that bamboo cellulose with a high length and aspect ratio improved the performance of the composite (Niu *et al.* 2021). In addition, the inherent biodegradability of cellulose and the tendency of cellulose to allow water into the interior of the bioplastic, such that it might have just the right rate of biodegradation, depending on what is expected. In this experiment, the authors prepared bamboo cellulose from bamboo residues and investigated the mechanism of alkali hydrolysis. The mechanical, barrier properties, and thermal properties related to the combination between cellulose, the γ-(2,3-epoxypropoxy) propytrimethoxysilane, and PBAT have not been studied previously.

In this present study, silanized cellulose/PBAT composite films with cellulose content were prepared by one-step composite and extrusion blowing. The silanized cellulose/PBAT composite films are referred to as a K-Cellulose/PBAT composite film in the following article. The effects of the K-Cellulose/PBAT weight ratio in the composite matrix on the microstructures, mechanical properties, barrier properties, thermal property, and hydrophobicity of the films were investigated.

EXPERIMENTAL

Materials and Methods

Material

Bamboo residues were provided by a bamboo processing plant in Guangdong Province, China. Bamboo powder passed through a 400-mesh screen to obtain and was dried in a drying oven at 105 ℃ to maintain quality for further using The PBAT polymer used was an Ecoflex® C1200 grade (purchased from BASF, Ludwigshafen, Germany) with melt flow index (MFI) of 2.5 to 4.5 (at 190 °C; 2.16 kg), density of 1.26 ± 0.01 g/cm^3, and melting point of 115 ± 5°C. The γ-(2,3-epoxypropoxy) propytrimethoxysilane (KH560) was obtained from Shanghai Yuanye Bio-Technology Co., Ltd. (Shanghai, China). Sodium hydroxide, acetic acid, and sodium chlorite were bought from Tianjin Sailboat Chemical Reagent Technology Co., Ltd. (Tianjin, China).

Preparation of the Films

Purification of bamboo powder

First, 25 g of bamboo powder were placed into 250 mL 4.0% of NaOH solution, and the suspension was mechanically stirred at 80 ℃ for 100 min. The mixture was left to stand at room temperature overnight and then filtered. It was washed with distilled water to remove hemicellulose, resin, and other substances until the NaOH was cleaned up to a pH value of 7 and finally put in a 60 ℃ oven for 12 h (Qian *et al*. 2017). After this, the method of conventional sodium chlorite was used for the removal of lignin. Then 24 g of dried bamboo powder after alkali treatment was placed into 780 mL of distilled water, with 9 g of sodium chlorite and 6 mL of glacial acetic acid, for 1 h in a 75 ℃ constant temperature water bath. Subsequently, this process was repeated five times, until the bamboo powder turned white. In the meantime, the bamboo fiber was washed with distilled water to neutral with distilled water after each operation. Finally, the bamboo powder was obtained by air drying.

In addition, to further study cellulose, the authors also prepared nanocellulose using bamboo powder. Bleached sulfate (kraft) pulp (18 g) was dissolved in deionized water (500 mL) and soaked for 24 h, and the pulp suspension was obtained with a distributor (30000 rpm/min for 10 min). TEMPO (10 mg) and sodium bromide (100 mg) were dissolved in deionized water and water bath for 15 min, then added to the pulp suspension for oxidation. The pH was kept in the 10 to 11 range (using 1 wt% sodium hydroxide). Sodium hypochlorite solution (10 wt%, 59.6 mL) was added to the slurry mixture for the oxidation step, the sodium hydroxide solution (1 wt%) was added at the same time and sonication dispersion was performed at 500 W for 15 min to keep the pH value of the hybrid solution at 10 to 11.

Silanization modification of bamboo powder

The pretreated bamboo powder was placed in 80 ℃ convection oven for 24 h and fully dried. Some amount of deionized water was adjusted with glacial acetic acid to form an aqueous solution with pH value of 3.5 to 5.5, and the compatibilizer KH560 (Yuanye Bio-Technology Co. Ltd., Shanghai, China) was diluted with the absolute ethyl alcohol to form a coupling agent solution at a 1:5 ratio. Under a high-speed mixer at 60 ℃, the coupling agent solution was evenly sprayed on the corresponding bamboo powder surface according to a certain proportion of ingredients and stirred evenly. Afterwards, the above reaction mixture was centrifuged to separate the silanized cellulose at 11000 rpm/min for 10 min to remove KH-560. Then, the surface-treated cellulose was placed in a 50 ℃ convection oven for 6 h and set aside.

Preparation of Composites

The fabrication of cellulose was performed using melt extrusion as per the procedure mentioned (Oliveira *et al*. 2017). Before processing, silanized cellulose was dried in a vacuum oven (~80 °C) for 12 h to remove the moisture due to its hydrophilic nature. The PBAT was placed in an oven (~ 80 °C) for 12 h.

The cellulose and PBAT were packaged in polyethylene bags (Roy *et al*. 2020) and kept at room temperature for at least 24 h to balance all the ingredients. The mixtures were mixed into cellulose/PBAT with the mixture using a double screw extruder twin-screw extruder (Zhongcheng Precision Testing Instrument Co., Ltd., Wuhan, China). The preparation process of the composite materials is shown in Fig. 1.

The temperatures within parts of the granulation machine from the feeding area to the mold area were 125, 130, 135, and 120 ℃. The screw speed was 20 to 25 rpm/min. The films were prepared using an extruded film blower film-blowing system (BL-6176 Floor Film Blower, Baolun Precision Testing Instrument Co., Ltd., Wuhan, China), and mold diameter of 30 mm. The blowing membrane conditions included the following: 30 rpm for 30 min, four heating zones of 110, 125, 135, and 145 ℃, and a blowing membrane mold of 135 ℃; screw speed 15 rpm/min and traction speed of 3.5 m/min. The film thickness was maintained at 40 to 50 μm by carefully adjusting the blow-up ratio (the ratio of the blow bubble diameter to that of the die diameter) and the absorption ratio (the ratio of the die outlet absorption velocity to the film velocity). The silanized cellulose/PBAT composite films were achieved by adding silanized cellulose at ratios of 0 wt%, 0.5 wt%, 1 wt%, 1.5 wt%, and 2 wt%.

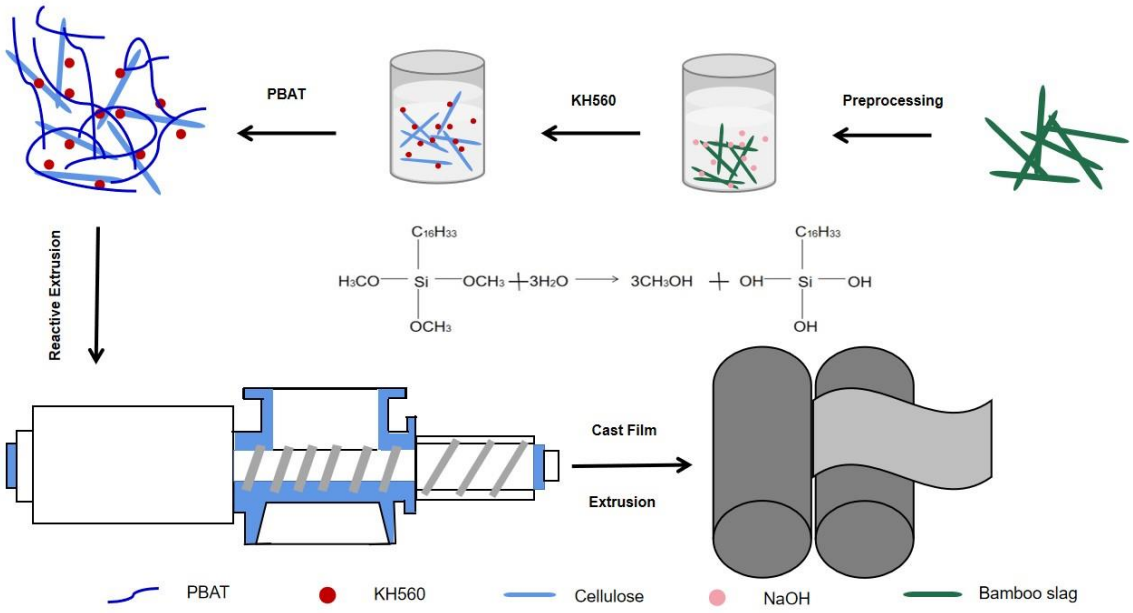

Fig. 1. Schematic illustration of the fabrication of composites

Preparation of Miscellaneous Straws

The suspension containing 3 g of cellulose (superfibers, nanofibers, or hybrid fibers) was fully mixed and filtered into a wet membrane using a 14-cm diameter funnel vacuum. The hybrid straws were prepared with different mixed amounts of nanocellulose and superfine cellulose.

Characterization of the Films

X-ray diffraction (XRD)

The crystal structures of cellulose and silanized cellulose were analyzed by X-ray diffraction using Cu Kα radiation (λ = 0.154 nm) with a scanning speed of 4°/min in scanning range of 10 to 80° (2θ) (Komal *et al*. 2020). The basal spacing of the nanoclay was calculated using the Bragg's diffraction equation, *i.e.*, $\lambda = 2d \cdot \sin\theta$, where λ is the wavelength of the X-ray radiation (0.1546 nm), d is the spacing between the diffraction lattice planes, and θ is the measured diffraction angle.

Fourier transformation infrared spectra (FTIR)

The FTIR analyses of cellulose modification with different concentrations of coupling agents (0%, 2%, 4%, 6%, and 8%) and silane cellulose composite membrane with varying concentrations of the cross-linking agent (0%, 0.5%, 1%, 1.5%, 2%, and 2.5%) were performed using a Nicolet 6700 spectrometer (Nicolet is5, ThermoFisher, Waltham, MA, USA) at ambient temperature. Data were collected over 16 scans at a 16 cm^{-1} resolution from 500 to 4000 cm^{-1} and analyzed using Origin 7.0 software (OriginLab Corporation, Northampton, MA, USA) (Si *et al*. 2020).

Scanning electron microscopy (SEM)

The surface and cross-sectional morphology of the films was observed with a scanning electron microscope (SEM, Hitachi, Tokyo, Japan) at a voltage of 2 kV (Wang *et al*. 2020a). Prior to examination, gold was coated on all the samples (Wang *et al*. 2020b). Film samples were frozen in liquid nitrogen and then cryofractured to obtain the cross-sectional samples. Images of the surface and cross-section were taken at magnifications of 500× and 2000×, respectively.

Static tensile test

Mechanical properties were tested according to the GB/T 1040 (2006). The mechanical properties of the films were tested at room temperature using an Instron 3369 (Norwood, MA, USA) universal testing machine. The size of the strip was 100 mm × 10 mm, and 8 samples were selected for testing. The distance between the upper and lower clamps was 30 mm, and the tensile rate was 400 mm/min during the experiment.

Thermogravimetric analysis (TGA)

The TG measurements (TGA-Q50, TA Instruments, New Castle, DE, USA) were performed using a thermal analysis system under the protection of the nitrogen atmosphere at a heating rate of 10 °C min^{-1} from 30 to 800 °C. During the measurement, dried nitrogen was vented into the furnace at a constant flow rate of 50 mL min^{-1} (Wang *et al*. 2005).

Differential scanning calorimetry (DSC)

The glass transition temperature of the composite film was determined using a DSC204F1 differential component thermometer (PerkinElmer, Waltham, MA, USA). The samples (approximately 5 mg to 10 mg) were subjected to two thermal cycles to observe the thermal behavior of the composites. In the first thermal cycle, the temperature was fixed from room temperature to 180 ℃ at 10 ℃/ min under the condition of N_2 protection and then held isothermally at 180 ℃ for 3 min to help remove the hot processing history. Afterwards, the temperature was reduced from 180 ℃ to 50 ℃ at 10 ℃/ min.

Water-vapor permeability (WVP)

The moisture permeability of film was tested according to the GB/T 1037-88 (2021) method of steam permeability test of plastic film and the sheet-cup method, the moisture permeability of silanized cellulose /PBAT blend packaging film was tested.

Oxygen permeability (OP)

The film's oxygen permeability system was determined by the GB/T 1038 (2000) pressure method of plastic film and sheet gas permeability test. The size of the sample was 150 mm × 150 mm, and three parallel samples were selected. The thickness of the film was

about 45 μm, based on measurement using a thickness gauge, and 5 points were averaged with a test temperature of 23 °C.

Water contact angle

The water contact angles of the films were measured by a VCA Optima dynamic contact angle tester (Optima, Hamburg, Germany) at room temperature. The films were first placed on the horizontal platform of the goniometer, and then a drop of deionized water (approximate 7 μL) was dropped onto the film using a precision microsyringe. Meanwhile, multiple photographs on the film of the water droplet were taken continuously for 150 s and stored. The valid values obtained were based on an average of at least five points. The changes in the contact angle of the film surface and the droplet tangent within 150 s were analyzed using appropriate software.

RESULTS AND DISCUSSION

XRD Analysis

The intercalated or exfoliated structures of composites can provide quantitative information through XRD analysis. Generally, according to the Bragg diffraction equation, the insertion of polymer molecules increases the d-spacing, resulting in the movement of the diffraction peak toward smaller angles.

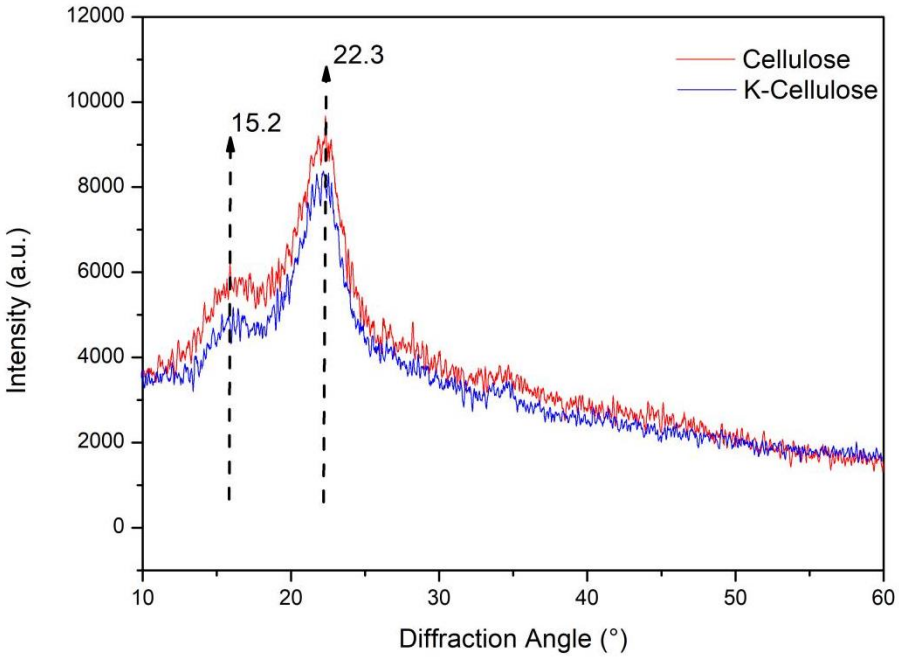

Fig. 2. XRD of cellulose and K- Cellulose

XRD analysis was used to characterize the crystallinity of cellulose and silanized cellulose samples, as demonstrated in Fig. 2. To all appearances, cellulose and silanized cellulose samples exhibited the well-known peaks at 14.9°, 16.7°, and 22.9°, which were mostly in agreement with the characteristic diffraction peaks of cellulose I. This result is consistent with the previous studies (Komal *et al*. 2020), meaning that the silanized

cellulose samples generally maintained the fundamental crystal structure of cellulose. However, there were still some subtle differences in the diffraction pattern. The diffraction peak intensity of silanized cellulose was reduced when compared to cellulose, indicating a reduced cellulose crystallinity after silanation modification. The reason for the reduced crystallinity can be because the surface of silanized cellulose was branched by the amorphous silanyl side groups (Robles *et al*. 2015).

FTIR Analysis

FTIR analysis can effectively study the molecular interactions that occur during reactive extrusion (Wei *et al*. 2021). Figure 3a depicts the FTIR spectra of cellulose and silanized cellulose samples. As a group, for cellulose and silanized cellulose samples, a strong band appeared at approximately 3408 cm^{-1}, which was mainly attributed to the stretching vibration of O-H groups. After the coupling agent modification, the telescopic vibration peak of the O-H group was weakened, indicating that the KH560 reacted with the O-H group in the cellulose and reduced the fiber polarity. The characteristic peak around 2890 cm^{-1} was largely associated with the -C=O stretching vibrations. Moreover, an intense adsorption around 1648 cm^{-1} originated from the absorbed water. Furthermore, the peaks at around 1374 cm^{-1} and 1065 cm^{-1} were related to $-CH_2$ and -C-H bending vibrations, respectively.

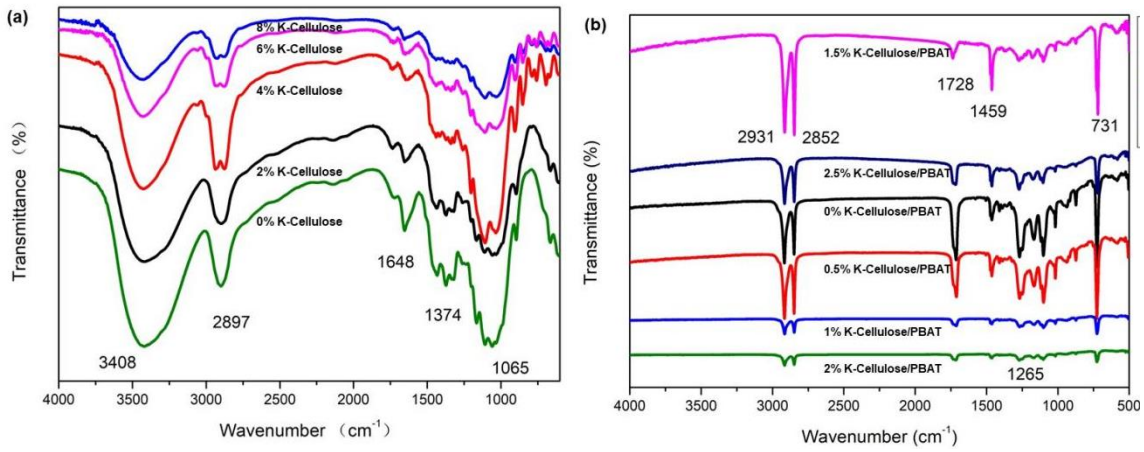

Fig. 3. FTIR spectra of Cellulose, K- Cellulose, and K-Cellulose/PBAT composite films

Figure 3b shows the FTIR spectra of the composite films with various weight proportions of silanized cellulose and PBAT. The PBAT belongs to the polyester family; hence it exhibited C-O stretching vibration peaks near 1265 cm^{-1}, which is characteristic of esters. Near 1459 cm^{-1} is the absorbance peak of C-H asymmetric and symmetrical bending vibrations. The broad peak around 3400 cm^{-1} occurred because of the presence of a large number of hydroxyl groups (−OH) in the starch chains (Fig. 3b). Compared with the pure PBAT, the position of the characteristic absorbance peak of the composite was basically unchanged, but the intensity of some absorbance peaks noticeably changed. Moreover, the strength of the stretching vibration peak near the 1459 cm^{-1} of the composite became stronger. This occurred because of the stretching vibration peaks of C-O-C and Si-O-C formed by silanized cellulose near 1459 cm^{-1} (Wu *et al*. 2019). The absorbance peak of C-H in alkanes was obviously enhanced, especially in the 1.5 wt% K-Cellulose/PBAT. The corresponding absorption intensity increased more noticeably, because the 0.5 wt% K-

Cellulose/PBAT, compared to 1.5 wt% K-Cellulose/PBAT silanization was highest, since it contains more alkanes.

Morphological SEM Analysis and Mechanical Properties

To intuitively describe and analyze the surface and cross-section morphology of the composites (Xing *et al*. 2020), the compatibility of the two phases of the composites was further studied by SEM.

The surface of the cellulose was smooth, while the K-Cellulose powders were rougher (Fig. 4). The surface showed distinct grooves that formed obvious pores that can produce a strong capillary effect (Yeo *et al*. 2020) and in turn can improve the infiltration effect of the plastic matrix, thus enhancing the interfacial forces between the PBAT and cellulose. Furthermore, the geometric average diameter of cellulose was approximately a few microns, while the diameter of K-Cellulose powders was increased to around 40 μm. These results were attributed to the effect of the interactions through hydrogen bonding, which leads to severe aggregation. After KH560 modification, the diameter of cellulose was further increased. With the dimensional changes, it was shown that the average diameter gradually increased for KH560-cellulose because of the introduction of grafting molecular chains on the cellulose surface.

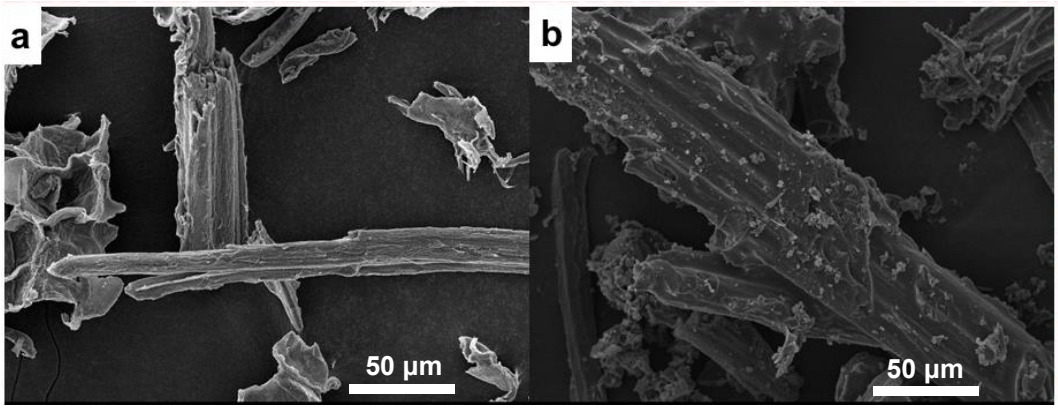

Fig. 4. SEM images of (a) Cellulose and (b) K-Cellulose

Figure 5 contains SEM micrographs of a liquid nitrogen fractured section of PBAT and its composites. The section of the PBAT was relatively flat, indicating PBAT brittle fracture occurred after liquid nitrogen treatment. There was little difference in cross-section morphology of 5 composites (Fig. 5), 0.5 wt%, 1 wt%, 1.5 wt%, 2 wt%, and 2.5 wt% K-Cellulose/PBAT. The cross-sections of the composites were flat, indicating that the dispersion of K-Cellulose in PBAT was better, because silanization modified the hydrophilic hydroxyl groups on cellulose molecular chains to be replaced by hydrophobic Si-O-C bonds (Zare and Rhee 2019), thus improving the interdependence of the two phases.

Cellulose and silane coupling agent were esterified in the course of reactive extrusion to connect nonpolar ester group to cellulose molecular chain, which will improve the interfacial compatibility between cellulose and PBAT and further affect the mechanical properties of the composites. In general, as the compatibility of the two phases is improved, the mechanical properties of the composites will be improved.

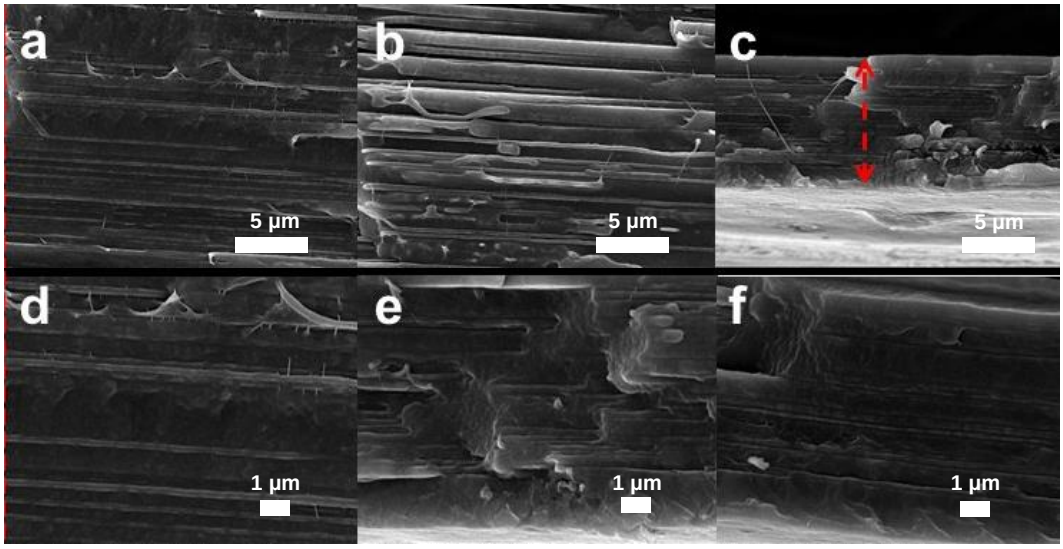

Fig. 5. SEM images of (a) 0 wt% K-Cellulose/PBAT, (b) 0.5 wt% K-Cellulose/PBAT, (c) 1 wt% K-Cellulose/PBAT, (d) 1.5 wt% K-Cellulose/PBAT, (e) 2 wt% K-Cellulose/PBAT, (f) 2.5 wt% K-Cellulose/PBAT

The mechanical properties of the composites were assessed by the mechanical analysis, as illustrated in Fig. 6. The tensile strength (TS), elongation at break (EB), and elastic modulus (MoE) of the K-Cellulose/PBAT composite with 2 wt% K-Cellulose content were increased by 1.8, 1.3, and 3.8 times, respectively, over the cellulose /PBAT blend without the added KH560. The higher toughening effect of KH560 in cellulose /PBAT composites can be mainly ascribed to the improved interfacial bonding between cellulose and PBAT. The γ-(2,3-epoxypropoxy) propytrimethoxysilane (KH560) can react with the hydroxyl group on the cellulose surface.

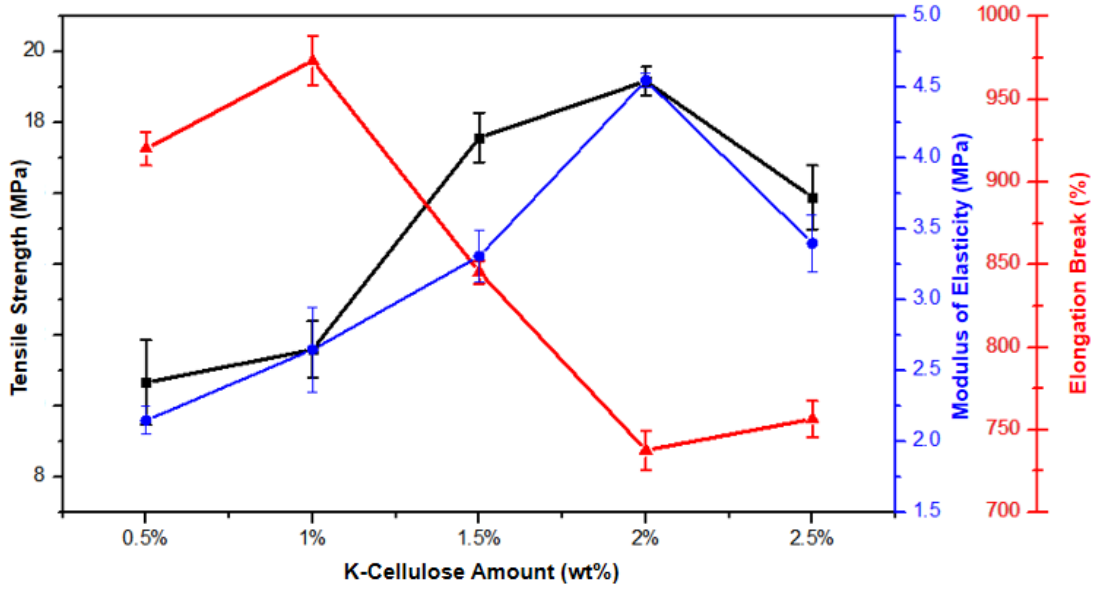

Fig. 6. TS, MoE, and EB of PBAT/ K-Cellulose films as a function of different K-Cellulose amounts

The elongation at break of the composite membrane showed a downward trend, and with the increase of silanized cellulose in the composite membrane, the elongation of the break increased first and then decreased and then slightly increased. A decrease in elongation at break by 11% was observed compared with that of 0.5%K-Cellulose/PBAT composite film when 2% silanized cellulose was added. The compatibility of the composites with different modified cellulose dosages is different, so it is necessary to test the mechanical properties of the composites with different modified cellulose dosages, select the appropriate blending ratio, and ensure the excellent mechanical properties of the composites.

The decrease in tensile strength of high-content of silanized cellulose of composite films can be mainly because of the agglomeration of excess K-Cellulose, resulting in a weaker interaction between particles and PBAT. Furthermore, the alkyl groups between the KH-560 molecules were poly-clustered and wound around the K-Cellulose surface reducing the contact area with the PBAT molecule. This reduces the effective interface layer and reduces the mechanical properties of the composite membrane.

TGA Analysis

The thermal properties of the obtained cellulose and silanized cellulose were assessed by TG-derivative thermogravimetry (DTG) analysis, as shown in Fig. 6(a,b). It can be observed in Fig. 6a that silanized cellulose slightly decreased weight at 300 °C and then exhibited a sharp weight loss at 300 to 500 °C.

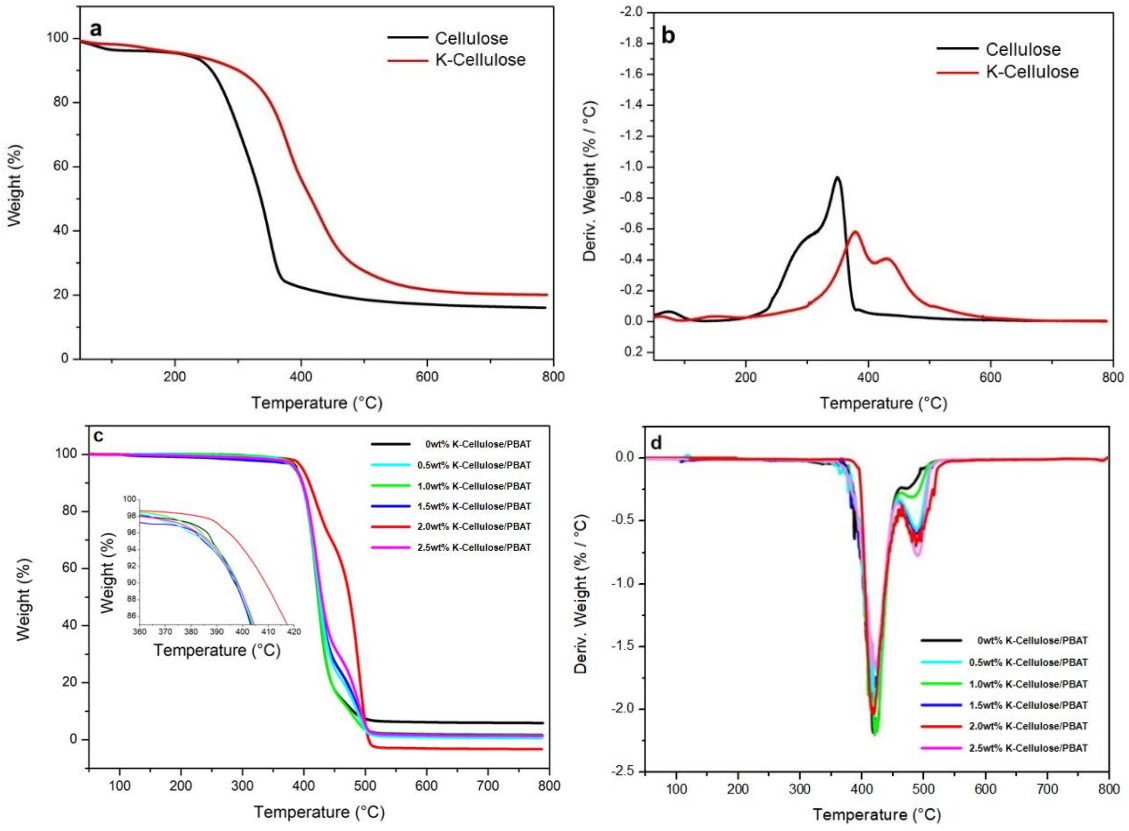

Fig. 7. (a,c) TG-curves and (b,d) DTG-curves of Cellulose, K-Cellulose, and PBAT/ K-Cellulose composite films

These results were similar to those reported in the previous works (Zhang *et al*. 2020). For silanized cellulose, there was a slight weight loss up to 350 °C, while the vast majority of weight loss occurred in the range of 350 to 500 °C. Furthermore, DTG peak temperature can also be used to evaluate the thermal stability of samples. According to the DTG curve in Fig. 6b, the initial weight thermal decomposition peaks occurred at 300 °C and 380 °C for cellulose and silanized cellulose, respectively. The above results provided direct evidence that the thermal stability of silanized cellulose samples was higher than that of cellulose. In addition, the amounts of the char residues for cellulose and silanized cellulose were 18% and 23%, respectively (Fig. 6a). The presence of alkoxysilane group may be the main reason to increase char residue for silanized cellulose samples. The thermal degradation start temperature in the silanized cellulose samples was higher than that of cellulose, indicating that the two-step modification method could improve the thermal stability of cellulose.

Thermogravimetric analysis was also used to characterize the effect of KH560 on the thermal stability of the composites. It was found that the TG decomposition temperature of the PBAT film was 364 ℃. After addition of KH560, the TG decomposition temperature of the composite increased from 363 to 395 ℃, improving by 30 ℃, indicating that the addition of silanized cellulose efficiently improved the thermal stability of silanized cellulose/PBAT composite. From Fig. 6d, it can be seen that there were two peaks. These double peaks are due to the degradation of the silanized cellulose/PBAT composite. The first is degradation of cellulose, at 356.7 ℃, the second is degradation of PBAT, at approximately 410.1 ℃. The two peaks were due to the uneven molecular structure, which contains some small molecular substances. In the process of heating, some crosslinked small molecules are destroyed, resulting in the loss of some raw materials. After adding 2% of silanized cellulose, the temperature of the two thermal degradation processes varied slightly. Because of the heterogeneity of molecular structure, the thermal degradation rate varied greatly with the addition of KH560.

KH560 acts as a chain amplicon in the mixing process (Zhang *et al*. 2020); thus, it not only accelerates the thermal movement between molecules and increases the molecular weight, but it also increases the binding force between chemical bonds, making it not easily destroyed at high temperature.

DSC Analysis

The crystallization and melting behavior of the K-Cellulose/PBAT composites were studied using DSC. The thermal history of the material will be removed during the first heating, and then followed by crystallization and subsequent thermal runs during cooling to study the melting behavior. The crystallization exotherms in the cool runs are shown in Fig. 7(a) and the second heat runs (melting endotherms) are shown in Fig. 7(b).

Clearly, the incorporation of the silanized cellulose in the PBAT matrix showed that the crystallization temperature of the matrix gradually increased towards higher temperatures. The observed T_c of 96 °C increased to 102 °C with incorporation of silanized cellulose particles. This clearly shows that the presence of the cellulose whiskers gave a heterogeneous nucleation effect (Zhou *et al*. 2020) through increasing the nucleating sites for promotion of crystallization of the PBAT where silicate platelets provided nucleating sites for the polymer matrix crystallization. In the second heating cycle (Fig. 7(b)), it can be seen that while the pure PBAT showed an endothermic melting peak at 117 °C. With increasing content of silanized cellulose, the melting temperatures showed a gradual increase up to the maximum temperature of 117 °C for the 1.5% silanized cellulose sample.

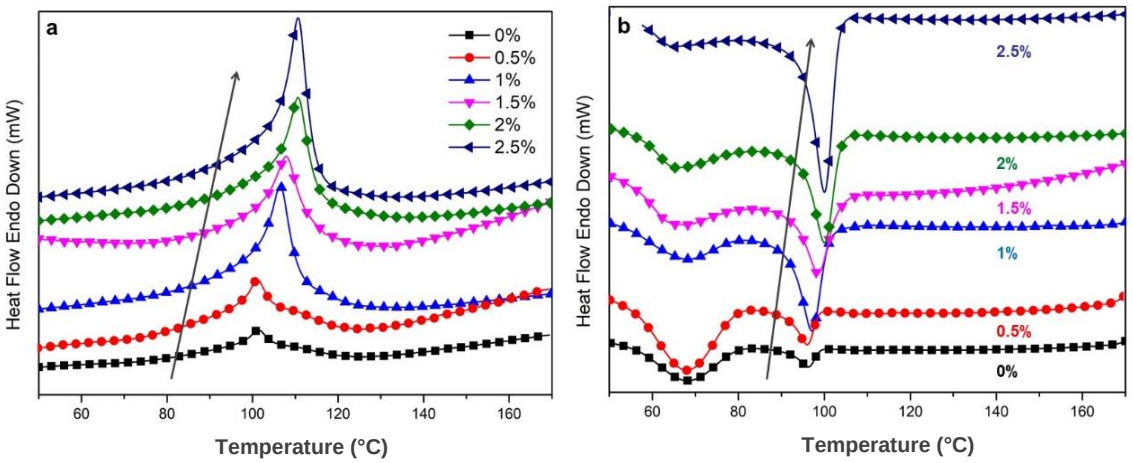

Fig. 8. DSC of PBAT/ K-Cellulose composite films with different amounts of K-Cellulose

Barrier Properties

The influence of silanized cellulose on barrier properties of films was investigated, and the WVP and OP values of all the film samples are illustrated in Table 1.

It can be observed that the PBAT film exhibited maximum WVP compared with the K-Cellulose/PBAT composite films. The K-Cellulose/PBAT composite films exhibited a reduction in WVP with the increase in the silanized cellulose content. The WVP of the 1.5 wt% K-Cellulose/PBAT composite film decreased to approximately one half that of the 0.5 wt% K-Cellulose/PBAT composite film. Cellulose is well known to be a hygroscopic material and has a greater affinity for water than PBAT. This property causes an increase in the permeability of water vapor through the films under high silanized cellulose content. Furthermore, the more intercalated structure has better compatibility in the film matrix with higher silanized cellulose content, which can contribute to a lower WVP.

Table 1. WVP and OP of the PBAT/ K-Cellulose Composite Films

Samples	WVP(g/(m^2.day))	OP(cm^3.m^{2}d bar)
PBAT	72.2408	4040
0.5% K-Cellulose /PBAT	58.3105	2150
1.0% K-Cellulose /PBAT	48.1428	1700
1.5% K-Cellulose /PBAT	29.8968	1370
2.0% K-Cellulose /PBAT	59.9336	1970
2.5% K-Cellulose /PBAT	76.5052	1440

In contrast to the WVP of the films, the OP values were reduced with increasing silanized cellulose content. In general, the factors that affect the OP of the films include microstructure, void volume, alignment of polymer chains, and adhesion of film matrix. The results are demonstrated in Table 1. When the silanized cellulose addition increased from 0 to 1.5 wt%, the air permeability decreased from 4040 to 1370 cm^3.m^{2}d bar. The results may be because the PBAT is composed of nonpolar molecules whose nonpolar oxygen molecules readily pass through the membrane matrix. The well-dispersed mixture allowed the composite membrane to form uniform and tight network structures, which may be in part responsible for the reduced air permeability. The addition of silanized cellulose

promoted the formation of an intercalated structure, which could prevent oxygen molecules from passing through the film matrix.

Surface Hydrophobicity

Water contact angle is the main indicator of the hydrophobic characterization of polymer materials. The contact angle of the PBAT/ K-Cellulose composite films were observed to further study the durability of hydrophobic characterization of polymer materials. The dynamic water contact angles of the film samples within 150 s are shown in Fig. 9. The water contact angle of the membrane decreases with time because of the reorientation of the membrane-surface polar group (Zhou *et al*. 2020). The images of the water droplet taken on the films explicitly reflected this phenomenon. The K-Cellulose/PBAT composite films also exhibited a small drop. In particular, the water contact angle of the 1.5 wt% K-Cellulose/PBAT composite film was only reduced 11° within 150 s after the water drop. The water contact angle of the 2 wt% K-Cellulose/PBAT composite film measured at 150 s was 39.8°, whereas the 1.5 wt% K-Cellulose/PBAT composite film exhibited higher water contact angles, especially the 1 wt% K-Cellulose/PBAT (76.2°) and 1.5 wt% K-Cellulose/PBAT (72.1°) composite films. Therefore, although the addition of silanized cellulose reduces the hydrophobicity of the composite film, the 1.5 wt% K-Cellulose/PBAT composite film did not decrease much compared to pure PBAT. This indicated that hydrophobization of the silanized cellulose was successfully achieved by KH560, and improvement of dispersibility in PBAT was expected.

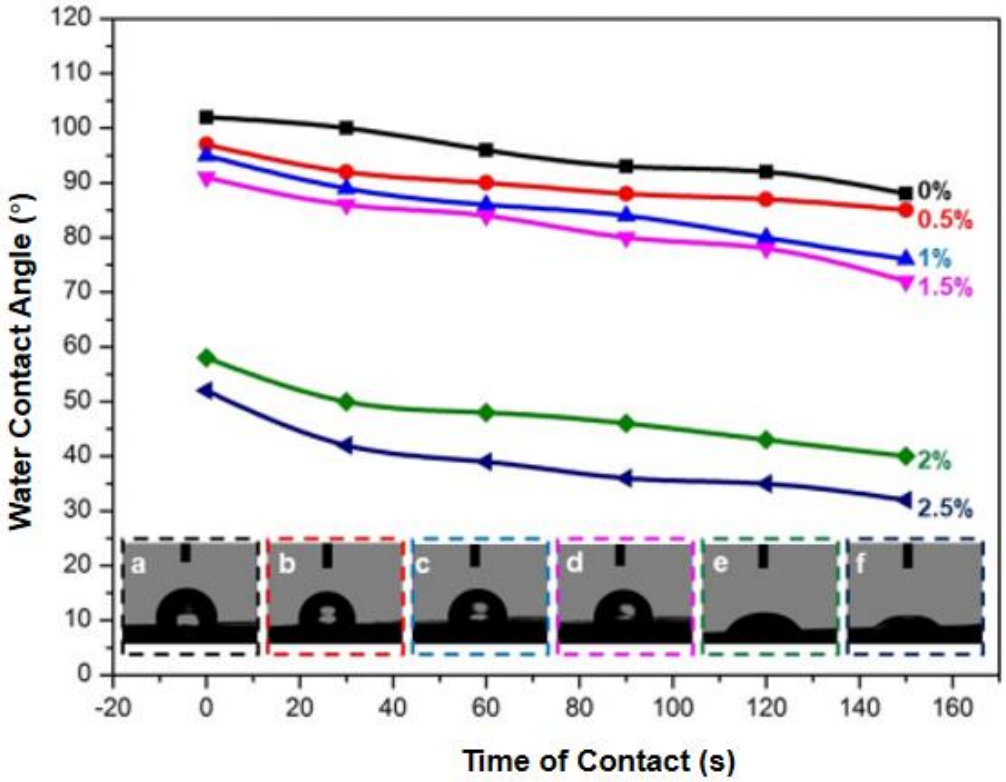

Fig. 9. Water contact angle of the PBAT/ K-Cellulose composite films

CONCLUSIONS

1. In the present work, bamboo-based cellulose was employed as a filler for poly(butyleneadipate-co-terephthalate) (PBAT) biocomposites, and KH560 as a compatibilizer of the composite membrane. K-Cellulose/PBAT composite membranes were successfully prepared by one-step compounding and subsequent extrusion blowing, and it was found that the composites prepared after the addition of modified cellulose had a good appearance and mechanical properties.
2. All formulations exhibited excellent processability. K-Cellulose/PBAT composites with 2 wt% silanized cellulose content had a relatively high level of transparency and tensile modulus; excessive silanized cellulose contents lowered the tensile property, such as K-Cellulose/PBAT composites with 2 wt% silanized cellulose. The SEM images of the composite films over a range with a continuous and uniform appearance with increasing silanized cellulose. These results showed that silanized cellulose is a good reinforcing material.
3. This work prepared different proportions of K-Cellulose/PBAT composite films by varying the silanized cellulose content, suggesting a green and feasible route to produce cost-efficient biodegradable materials for packaging applications. These results indicate that K-Cellulose/PBAT composite, as a fully degradable composite film, has a great potential in food packaging materials, which can reduce the use of non-biodegradable plastics and alleviate environmental problems.

ACKNOWLEDGEMENTS

This work was supported by the Tianjin Enterprise Science and Technology Commissioner Project (21YDTPJC00570).

REFERENCES CITED

Adam, J., Korneliusz, B. A., and Agnieszka, M. (2013). "Dynamic mechanical thermal analysis of biocomposites based on PLA and PHBV-A comparative study to PP counterparts," *Journal of Applied Polymer Science* 130(5), 3175-3183. DOI: 10.1002/app.39562

Bodros, E., Pillin, I., Montrelay, N., and Baley, C. (2007). "Could biopolymers reinforced by randomly scattered flax fibre be used in structural applications?," *Composites Science and Technology* 67(3-4), 462-470. DOI: 10.1016/j.compscitech.2006.08.024

Cao, J., Zhou, Z., Song, Q., Chen, K., Su, G., Zhou, T., Zheng, Z., Lu, C., and Zhang, X. (2020). "Ultrarobust Ti3C2Tx MXene-based soft actuators *via* bamboo-inspired mesoscale assembly of hybrid nanostructures," *ACS Nano* 14(6), 7055-7065. DOI: 10.1021/acsnano.0c01779

Da Costa, M. C. F., Souza, M. R. M., and Larrude, D. R. G. (2019). "Adhesion between graphene and polymers: a surface analysis perspective," *Express Polymer Letters* 13, 52-64. DOI: 10.3144/expresspolymlett.2019.6

Darshan, T. G., Veluri, S., Kartik, B., Yen-Hsiang, C., and Fang-Chyou, C. (2019). "Poly(butylene succinate)/high density polyethylene blend-based nanocomposites with enhanced physical properties – selectively localized carbon nanotube in pseudo-double percolated structure," *Polymer Degradation and Stability* 163, 185-194. DOI: 10.1016/j.polymdegradstab.2019.03.009

Edlund, U., Lagerberg, T., and Alander, E. (2019). "Admicellar polymerization coating of CNF enhances integration in degradable nanocomposites," *Biomacromolecules* 20(2), 684-692. DOI: 10.1021/acs.biomac.8b01318

Fukushima, K., Wu, M. H., Bocchini, S., Rasyida, A., and Yang, M. C. (2012). "PBAT based nanocomposites for medical and industrial applications," *Materials Science and Engineering: C* 32(6), 1331-1351. DOI: 10.1016/j.msec.2012.04.005

Higbee-Dempsey, E. M., Amirshaghaghi, A., Case, M. J., Bouche, M., Kim, J., and Cormode, D. P. (2020). "Biodegradable gold nanoclusters with improved excretion due to pH-triggered hydrophobic-to-hydrophilic transition," *Journal of the American Chemical Society* 142(17), 7783-7794. DOI: 10.1021/jacs.9b13813

Jin, X., Zhang, X., Xu, C., and Nie, S. (2019). "Effect of bamboo fibers with different coupling agents on the properties of poly(hydroxybutyrate-co-valerate) biocomposites," *Journal of Applied Polymer Science* 136(20), article ID 47533. DOI: 10.1002/app.47533

Kim, J. W., and Cho, J. U. (2020). "Fracture properties on the adhesive interface of double cantilever beam specimens bonded with lightweight dissimilar materials at opening and sliding modes," *Composites Part B: Engineering* 198, article ID 108240. DOI: 10.1016/j.compositesb.2020.108240

Komal, Kanu Gupta, K., Kumar, V., Tikoo, K. B., Kaushik, A., and Singhal, S. (2020). "Encrustation of cadmium sulfide nanoparticles into the matrix of biomass derived silanized cellulose nanofibers for adsorptive detoxification of pesticide and textile waste," *Chemical Engineering Journal* 385(123700), 1385-8947. DOI: 10.1016/j.cej.2019.123700

Li, X., Liu, P., Mao, Y., Xing, M. Y., and Zhang, J. L. (2015). "Preparation of homogeneous nitrogen-doped mesoporous TiO_2 spheres with enhanced visible-light photocatalysis," *Applied Catalysis B: Environmental* 164, 352-359. DOI: 10.1016/j.apcatb.2014.09.053

Lin, W., Hu, X., You, X., Sun, Y. Y., Wen, Y. Q., Yang, W. B., Zhang, X. X., Li, Y., and Chen, H. X. (2018). "Hydrophobic modification of nanocellulose *via* a two-step silanation method," *Polymers (Basel)* 10(9), article 1035. DOI: 10.3390/polym10091035

Mhd Ramle, S. F., Ahmad, N. A., Mohammad Rawi, N. F., Zahidan, N. S., and Geng, B. J. (2020). "Physical properties and soil degradation of PLA/PBAT blends film reinforced with bamboo cellulose," *IOP Conference Series: Earth and Environmental Science* 596, article ID 012021. DOI: 10.1088/1755-1315/596/1/012021

Niu, S., Zhang, X., Williams, G. R., Wu, J., Gao, F., Fu, Z., Chen, X., Lu, S., and Zhu, L. M. (2021). "Hollow mesoporous silica nanoparticles gated by chitosan-copper sulfide composites as theranostic agents for the treatment of breast cancer," *Acta Biomaterialia* 126, 408-420. DOI: 10.1016/j.actbio.2021.03.024

Qian, S. P., Zhang H. H., and Sheng K. C. (2017). "Cellulose nanowhiskers from moso bamboo residues: Extraction and characterization," *BioResources* 12, 419-433. DOI: 10.15376/biores.12.1.419-433

Oliveira, T. A., Oliveira, R. R., Barbosa, R., Azevedo, J. B., and Alves, T. S. (2017). "Effect of reprocessing cycles on the degradation of PP/PBAT-thermoplastic starch blends," *Carbohydrate Polymers* 168, 52-60. DOI: 10.1016/j.carbpol.2017.03.054

Robles, E., Urruzola, I., Labidi, J., and Serrano, L. (2015). "Surface-modified nano-cellulose as reinforcement in poly(lactic acid) to conform new composites," *Industrial Crops and Products* 71, 44-53. DOI:10.1016/j.indcrop.2015.03.075

Roy, P., Defersha, F., Rodriguez-Uribe, A., Misra, M., and Mohanty, A. K. (2020). "Evaluation of the life cycle of an automotive component produced from biocomposite," *Journal of Cleaner Production* 273, article ID 123051. DOI: 10.1016/j.jclepro.2020.123051

Si, W.-J., Zhang, H., Li, Y.-D., Huang, C., Weng, Y.-X., and Zeng, J.-B. (2020). "Highly toughened and heat resistant poly(l-lactide)/poly(ε-caprolactone) blends *via* engineering balance between kinetics and thermodynamics of phasic morphology with stereocomplex crystallite," *Composites Part B: Engineering* 197, article ID 108155. DOI: 10.1016/j.compositesb.2020.108155

Wang, Y., Rodriguez-Perez, M. A., Reis, R. L., and Mano, J. F. (2005). "Thermal and thermomechanical behaviour of polycaprolactone and starch/polycaprolactone blends for biomedical applications," *Macromolecular Materials and Engineering* 290(8), 792-801. DOI: 10.1002/mame.200500003

Wang, D., Wang, Q., and Huang, Z. (2020a). "New insights into the early reaction of NaOH-activated slag in the presence of $CaSO_4$," *Composites Part B: Engineering* 198, article ID 108207. DOI: 10.1016/j.compositesb.2020.108207

Wang, H.-M., Wang, B., Yuan, T.-Q., Zheng, L., Shi, Q., Wang, S. F., Song, G.-Y., and Sun, R.-C. (2020b). "Tunable, UV-shielding and biodegradable composites based on well-characterized lignins and poly(butylene adipate-co-terephthalate)," *Green Chemistry* 22(24), 8623-8632. DOI: 10.1039/d0gc03284k

Wei, X. F., Bohlen, M., Lindblad, C., Hedenqvist, M., and Hakonen, A. (2021). "Microplastics generated from a biodegradable plastic in freshwater and seawater," *Water Research* 198, article ID 117123. DOI: 10.1016/j.watres.2021.117123

Wu, T., Cai, B., Wang, J., Zhang, C. G., Zhang, Z. Q., Yang, Q. L., Hu, G.-H., and Xiong, C. (2019). "TEMPO-oxidized cellulose nanofibril/layered double hydroxide nanocomposite films with improved hydrophobicity, flame retardancy and mechanical properties," *Composites Science and Technology* 171, 111-117. DOI: 10.1016/j.compscitech.2018.12.019

Yeo, J. C. C., Muiruri, J. K., Koh, J. J., Thitsartarn, W., Zhang, X., Kong, J., Lin, T. T., Li, Z., and He, C. (2020). "Bend, twist, and turn: First bendable and malleable toughened PLA green composites," *Advanced Functional Materials* 30(30), article ID 2001565. DOI: 10.1002/adfm.202001565

Zare, Y., and Rhee, K. Y. (2019). "Following the morphological and thermal properties of PLA/PEO blends containing carbon nanotubes (CNTs) during hydrolytic degradation," *Composites Part B: Engineering* 175, article ID 107132. DOI: 10.1016/j.compositesb.2019.107132

Zhang, C., Gong, J., Li, H., and Zhang, J. (2020). "Fiber-based flexible composite with dual-gradient structure for sound insulation," *Composites Part B: Engineering* 198, article ID 108166. DOI: 10.1016/j.compositesb.2020.108166

Zhou, L., Liu, Z., Guan, Z., Tian, B., Wang, L., Zhou, Y., Zhou, Y., Lei, J., Zhang, J., and Liu, Y. (2020). "0D/2D plasmonic Cu2-xS/g-C3N4 nanosheets harnessing UV-vis-NIR broad spectrum for photocatalytic degradation of antibiotic pollutant," *Applied Catalysis B: Environmental* 263, article ID 118326. DOI: 10.1016/j.apcatb.2019.118326

Article submitted: October 24, 2022; Peer review completed: December 21, 2022; Revised version received January 3, 2023; Accepted: January 12, 2023; Published: January 24, 2023.
DOI: 10.15376/biores.18.1.1916-1932